Ligand Binding Determinants for Angiotensin II Type 1 Receptor from Computer Simulations

ARTICLE *in* JOURNAL OF CHEMICAL INFORMATION AND MODELING · OCTOBER 2013

Impact Factor: 3.74 · DOI: 10.1021/ci400400m · Source: PubMed

5 AUTHORS, INCLUDING:

Minos Matsoukas
Cloudpharm
19 PUBLICATIONS **162** CITATIONS
SEE PROFILE

Arnau Cordomi
Autonomous University of Barcelona
47 PUBLICATIONS **474** CITATIONS
SEE PROFILE

Santiago Rios Azuara
Autonomous University of Barcelona
2 PUBLICATIONS **8** CITATIONS
SEE PROFILE

Leonardo Pardo
Autonomous University of Barcelona
114 PUBLICATIONS **3,773** CITATIONS
SEE PROFILE

JOURNAL OF CHEMICAL INFORMATION AND MODELING

Article

pubs.acs.org/jcim

Ligand Binding Determinants for Angiotensin II Type 1 Receptor from Computer Simulations

Minos-Timotheos Matsoukas,[†,‡] Arnau Cordomí,[‡] Santiago Ríos,[‡] Leonardo Pardo,[‡] and Theodore Tselios*[,†]

[†]Department of Chemistry, University of Patras, GR-26504, Rion, Patras, Greece

[‡]Laboratori de Medicina Computacional, Unitat de Bioestadistica, Facultat de Medicina, Universitat Autonoma de Barcelona, E-08193, Bellaterra, Barcelona, Spain

Supporting Information

ABSTRACT: The ligand binding determinants for the angiotensin II type 1 receptor (AT_1R), a G protein-coupled receptor (GPCR), have been characterized by means of computer simulations. As a first step, a pharmacophore model of various known AT_1R ligands exhibiting a wide range of binding affinities was generated. Second, a structural model of AT_1R was built making use of the growing set of crystal structures of GPCRs, which was further used for the docking of the AT_1R ligands based on the devised pharmacophore model. Next, ligand−receptor−lipid bilayer systems were studied by means of molecular dynamics (MD) simulations. Overall, the present study has permitted, combining the pharmacophore model with binding free energy calculations obtained from the MD simulations, to propose the molecular mechanisms by which sartans interact with AT_1R.

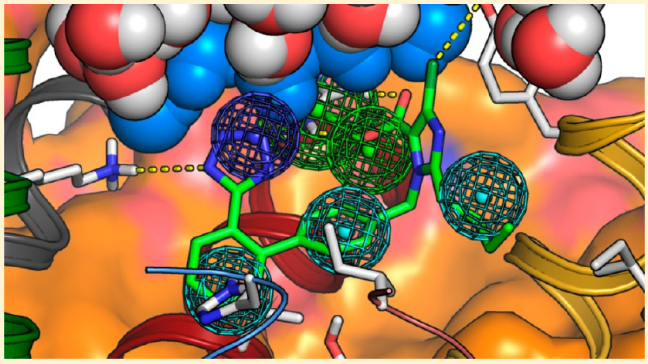

INTRODUCTION

The actions of the natural ligand angiotensin II, an octapeptide that is a RAAS (renin−angiotensin−aldosterone-system) mediator, are elicited through specific G-protein coupled receptors (GPCRs) such as the angiotensin II receptor type 1 (AT_1R) and 2 (AT_2R) present on various target organs.[1] The most characteristic aftermaths of AT_1R are vasoconstriction, aldosterone and vasopressin release, sodium and water retention, left ventricular hypertrophy, and nephrosclerosis, making it an important target for drug development.[2] AT_2R has a less critical role in the aforementioned processes, but fine-tunes the regulation of natriuresis, body temperature, and blood pressure.[3]

Several orally administered potent nonpeptide antagonists targeting AT_1R, known as sartans, have been developed in the past as antihypertensive drugs, which regulate blood pressure in the human organism.[4] A vast number of compounds has also been recently reported.[5,6] Losartan, eprosartan, valsartan, irbesartan, candesartan, telmisartan, zolasartan, olmesartan, and saprisartan are clinically available AT_1R blockers for treatment of hypertension, diabetic nephropathy, and (or at risk) heart failure following myocardial infraction.[7] Depending on the dissociation rate of these antagonists from AT_1R, they are classified as noncompetitive, competitive surmountable, or competitive insurmountable.[8] EXP3174, the active metabolite of losartan with increased binding affinity relative to the latter, has been proven to be an inverse agonist such as olmesartan and candesartan.[9] Azilsartan,[10] a recently developed AT_1R antagonist, has just been approved for clinical use, and two additional compounds[11,12] are in the final stage of clinical trials, which reinforce the importance of AT_1R as a drug target.

Significant advances in crystallization of GPCRs[13,14] have permitted to elucidate the crystal structures of many receptors in the last years (see Katritch et al.[15,16] for recent reviews). All these structures share the common architecture of seven plasma membrane-spanning (or transmembrane) domains (TMs, which also terms this family of proteins as 7TM receptors) connected to each other with three extracellular (ECL) and three intracellular loops (ICL), a disulfide bridge between ECL 2 and TM 3, and a cytoplasmic C−terminus containing an α-helix (Hx8) parallel to the cell membrane.[17] The crystal structure of AT_1R is not solved, which obviates the building of AT_1R homology models from homologous proteins of known structure and similar sequence (templates). Because membrane proteins exhibit a strong conservation of the TM structure even at low sequence identity (<20%),[18] it is feasible to obtain an accurate homology model of AT_1R from the crystal structures of other GPCRs.

A pharmacophore definition is often the first essential step toward understanding the interaction between a ligand and its target receptor, and it is clearly established as a successful computational tool for rational drug design. The model developed during this work implements a pharmacophore model of known AT_1R ligands with a wide range of binding affinities, and molecular models of the ligand−receptor−lipid

Received: July 8, 2013

   dx.doi.org/10.1021/ci400400m | J. Chem. Inf. Model. XXXX, XXX, XXX−XXX

Table 1. Chemical Structures and K_i Values for the AT_1R Antagonists Used As Training Set in the Generation of the Pharmacophore Model for AT_1R Antagonists

Compound	Structure	K_i (nM)	Compound	Structure	K_i (nM)
c1	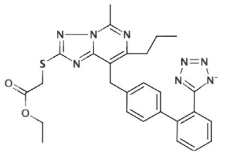	99[57]	c13	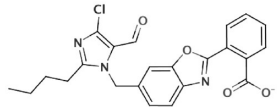	6100[58]
c2	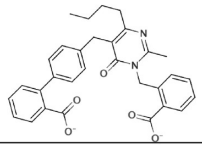	401[59]	c14	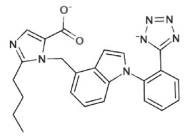	3600[58]
c3	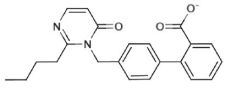	1097[59]	losartan	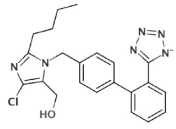	5[60]
c4	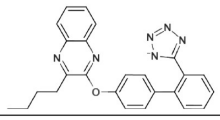	2200[61]	eprosartan	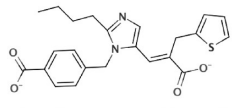	8.29[62]
c5	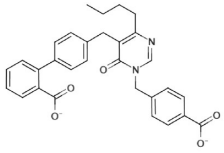	5317[59]	EXP3174	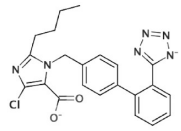	1.76[63]
c6	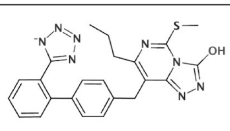	9000[57]	valsartan	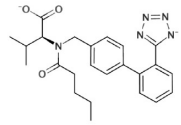	8.21[64]
c7	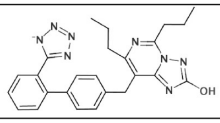	659[57]	irbesartan	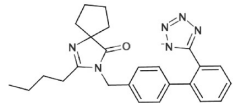	0.80[65]
c8	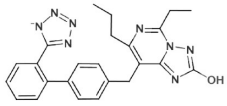	225[57]	olmesartan	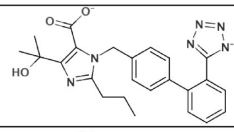	0.70[66]
c9	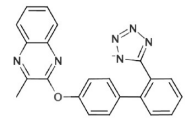	3450[61]	V8001	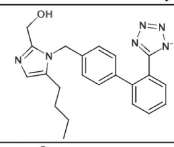	25[60]
c10	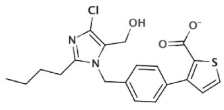	14500[67]	V8002	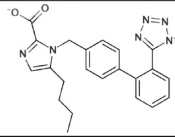	2.5[60]
c11	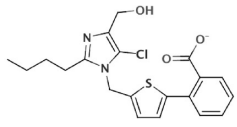	11600[67]	V8003	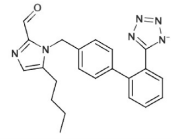	20[60]
c12	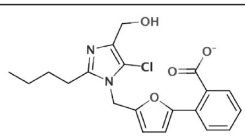	9700[67]	V8004	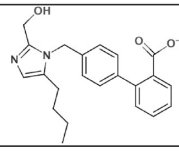	204[60]

bilayer system, which were obtained from homology modeling, docking, and molecular dynamics (MD) simulations. In addition, the experimentally obtained ligand-binding free energies are compared with the theoretically calculated, using the linear

dx.doi.org/10.1021/ci400400m | J. Chem. Inf. Model. XXXX, XXX, XXX−XXX

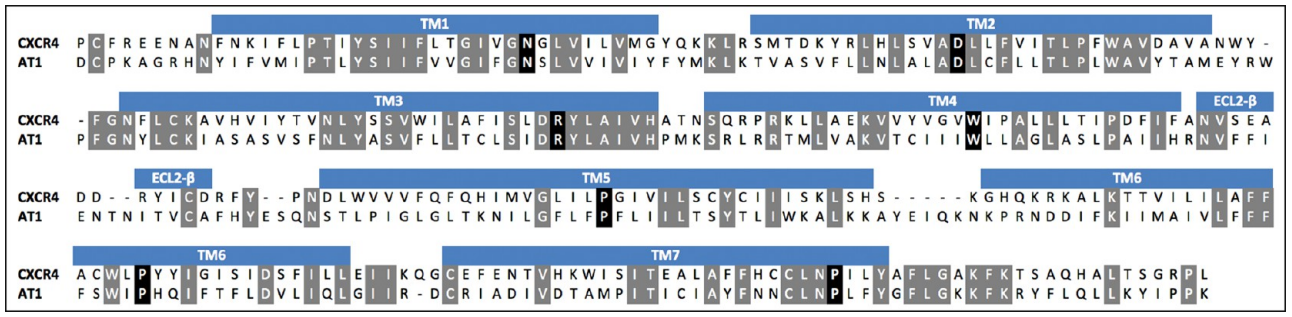

Figure 1. Sequence alignment of CXCR4 (Uniprot code: P61073) and the human AT_1R (Uniprot code: P30556). The key residues used for the alignment of TM helices are shown in black, and conserved amino acids are shown in gray. Regions corresponding to TM helices or β-strands (in ECL2) of the CXCR4 crystal structure (PDB id: 3ODU) are highlighted in blue.

interaction energy (LIE) method.[19] This combined computational study has permitted to propose the molecular mechanisms by which sartans interact with the AT_1R.

METHODS

A 3-D Pharmacophore Model. The pharmacophore model for AT_1R antagonists was generated with the Hypogen module of Discovery Studio[20] using the BEST conformational analysis procedure. Twenty-four structurally diverse compounds (Table 1) were built *de novo* using standard options within the 2D/3D editor sketcher of the program. Most of the selected compounds contain a tetrazole group or/and a carboxyl group, which have similar pK_a values of 4.89 and 4.76 respectively. Accordingly, the tetrazole and carboxyl groups were considered to be deprotonated in the environment of the receptor.[21] The number of conformers was limited to a maximum of 250 and restricted to those above a threshold of 20 kcal/mol relative to the global minimum. Four distinct chemical features were considered for hypothesis generation: hydrogen bond acceptor (HBA), hydrogen bond donor (HBD), hydrophobic (HYD), and negative ionizable (NI). The selection of the hypothesis was done based on a cost analysis procedure.[22] The two best output hypotheses (hypotheses 1 and 2), selected for description in the manuscript, are robust against statistical tests. The difference of 59.7 and 58.3 bits for hypotheses 1 and 2, respectively, between Fixed and Null Costs indicate a 90% chance of obtaining predictive hypotheses. These pharmacophore models were further validated for statistical significance using the Fischer randomization methods, in which the K_i values were scrambled randomly 49 times, and new hypotheses were generated (not shown). None of the outcome hypotheses had a cost lower than the reported hypothesis. Thus, there is at least 98% probability that these hypotheses represent true correlation in the data.

Computational Model of AT_1 Receptor. MODELLER v9.7[23] was used to build a homology model of human AT_1R (Uniprot code P30556) using the crystal structure of human CXCR4 (PDB code 3ODU)[24] as template. The highly conserved $N^{1.50}$ in TM 1, $D^{2.50}$ in TM 2, $R^{3.50}$ in TM 3, $W^{4.50}$ in TM 4, $P^{5.50}$ in TM 5, $P^{6.50}$ in TM 6, and $P^{7.50}$ in TM 7, which define the Ballesteros and Weinstein numbering scheme,[25] were used as reference points in TM sequence alignment (Figure 1).

Docking of AT_1 Receptor Antagonists. All docking runs were carried out with GOLD v5.2, using the Genetic Algoritm and the Goldscore and Chemscore scoring functions.[26] The selected docking solutions were rescored using the scoring functions implemented in Discovery Studio v.3.5[20] (LigScore1-Dreiding, LigScore2-Dreiding,[27] PLP1,[28] PLP2,[29] Jain,[30] and PMF[31]).

Molecular Dynamics Simulations. MD simulations of the ligand−receptor complexes were performed using the GROMACS software v4.5.3.[32] The complexes were embedded in a pre-equilibrated box ($9 \times 9 \times 10$ nm) containing a lipid bilayer (190 molecules of POPC) with explicit solvent (~13,000 water molecules) and a 0.15 M concentration of Na^+ and Cl^- ions (~130 ions) with its long axis perpendicular to the membrane interface.[33] Model systems were energy minimized and subsequently subjected to a 0.5 ns MD equilibration, with positional restraints on AT_1R Cα atoms. These restraints were released, and 5 ns MD trajectories were produced. All simulations were run at a constant temperature of 300 K using separate v-rescale thermostats[34] for the protein, ligand, lipids, and solvent molecules. A time step of 2 fs was used for the integration of equations of motion. All bonds and angles were kept frozen using the LINCS algorithm.[35] Lennard-Jones interactions were computed using a cutoff of 10 Å, and the electrostatic interactions were treated using PME[36] with the same real-space cutoff. The AMBER99SB-ILDN[37] force field was used for the protein, the parameters described by Berger and coworkers for the lipids,[38] and the general Amber force field (GAFF) and HF/6-31G*-derived RESP atomic charges for the ligands.[39] This combination of protein and lipid parameters has recently been validated.[40]

Quantum Mechanical Calculations. To discern the most energetically favored conformation of AT_1 receptor antagonists, quantum mechanical calculations at the B3LYP/6-31G* level of theory were performed using the torsional angle C12−C7−C4−C5 between the two phenyl rings (see Figure S1), which defines the *syn* and *anti* conformations of the ligands, as a reaction coordinate. All calculations were performed with the GAUSSIAN09 program.[41]

Linear Interaction Energy Calculations. According to the LIE approximation[19] the binding free energy (ΔG_{bind}^{LIE}) can be computed as

$$\Delta G_{bind}^{LIE} = \alpha \Delta \langle U_{l\text{-}s}^{vdW} \rangle + \beta \Delta \langle U_{l\text{-}s}^{el} \rangle + \gamma \quad (1)$$

where $\Delta \langle U_{l\text{-}s}^{vdW} \rangle$ and $\Delta \langle U_{l\text{-}s}^{el} \rangle$ account respectively for the average difference in van der Waals and electrostatic energies for the receptor-bound and for the free ligand. Coefficients α and β depend on the chemical nature of the ligands, whereas γ is a constant term that needs to be considered for calculations of absolute binding free energies.[19,42] Previously reported values of 0.18 and 0.5 for α and β respectively were used.[42,43] The receptor-bound potential energy terms were taken directly from the structures collected during the last 1 ns of each ligand/AT_1R simulation. The free ligand terms were obtained from additional

dx.doi.org/10.1021/ci400400m | J. Chem. Inf. Model. XXXX, XXX, XXX−XXX

2 ns MD simulations performed with the ligand in a water box using a similar simulation setup as for ligand/AT_1R systems. The computed binding free energies were obtained through the g_lie tool of GROMACS. Comparison to experimental binding free energies was made using either the $\Delta G^{exp}_{bind} = RTlnK_i$ relationship (for ligands with known K_i values) or the $\Delta G^{exp}_{bind} = RTln(IC_{50}) - RTln\ (1 + S/K_M)$ relationship (for ligands with known IC_{50} values).[44]

RESULTS AND DISCUSSION

A 3-D Pharmacophore Model for AT_1 Receptor Antagonists. Using the Hypogen algorithm (see Methods) we have developed a 3-D pharmacophore model from a set of 24 structurally diverse AT_1R antagonists with K_i values spanning from 0.7 to 14500 nM (Table 2). The two best pharmacophore hypotheses, hypothesis 1 (Figure 2A) and hypothesis 2 (Figure 2B), both contain five chemical features: a negatively ionizable group (NI), a hydrogen bond acceptor group (HBA), and three hydrophobic sites (HYD1-HYD3). The only difference between the two hypotheses is the location of NI, which is either in close proximity (hypothesis 1, Figure 2A) or distant (hypothesis 2, Figure 2B) to HBA. Table 2 shows the relation between experimental and predicted antagonistic activity for hypotheses 1 and 2. These models were further evaluated for statistical significance using the Fischer method (see Methods). In detail, losartan (Figures 2C and 2D) fulfills the NI feature through the tetrazole ring, the HBA match with an electronegative group located at the opposite side of the molecule, two of the HYD features match with the aromatics rings, and the third HYD feature corresponds to the hydrophobic chain. Losartan fits into hypothesis 1 with the NI and HBA elements in the *syn* conformation and into hypothesis 2 with these pharmacophore elements in the *anti* conformation. Several of the selected compounds contain a tetrazole (as NI) and a carboxyl group (as HBA) in their structure (Table 1), which are both deprotonated in the environment of the receptor as shown from the acid−base equilibrium constants of valsartan (see Methods).[21] We used *ab initio* calculations to evaluate the relative energy difference between the *syn* (hypothesis 1) and *anti* (hypothesis 2) conformations for losartan (see Methods), which contains only the negatively charged tetrazole group, and EXP3174, which containing two negatively charged groups (tetrazole and carboxyl groups). In losartan the *syn* conformation is 8.1 kcal/mol more stable than the *anti* conformation (due to the intramolecular hydrogen bond present between the tetrazole and the hydroxyl group). In contrast, the *anti* conformation is 0.7 kcal/mol more stable than the *syn* conformation in EXP3174 (due to the repulsion between the negatively charged groups in the latter) (Figure S1), showing that EXP3174 can exist in both conformations.

Table 2. Fit Scores and Comparison between Experimental and Estimated pK_i Values in the Training Set for Pharmacophore Hypotheses 1 and 2 (See Figure 2)[a]

	hypothesis 1				hypothesis 2			
		pK_i				pK_i		
compound	fit	est	exp	error	fit	est	exp	error
olmesartan	14.5	8.7	9.2	0.5	12.50	7.8	9.2	1.4
irbesartan	14.7	8.9	9.1	0.2	13.80	9.1	9.1	0
EXP3174	14.4	8.5	8.7	0.2	13.27	8.6	8.7	0.1
V8002	14.4	8.5	8.6	0.1	12.47	7.8	8.6	0.8
losartan	13.9	8.1	8.3	0.2	11.67	7.0	8.3	1.3
valsartan	13.5	7.7	8.1	0.4	13.19	8.5	8.1	−0.4
eprosartan	11.5	5.7	8.1	2.4	10.98	6.3	8.1	1.8
V8003	13.1	7.3	7.7	0.4	12.27	7.6	7.7	0.1
V8001	13.0	7.2	7.6	0.4	12.53	7.8	7.6	−0.2
C1	12.1	6.2	7.0	0.8	11.20	6.5	7.0	0.5
V8004	12.6	6.7	6.7	0	10.85	6.1	6.7	0.6
C8	12.1	6.3	6.7	0.4	12.05	7.3	6.7	−0.6
C2	12.5	6.6	6.4	−0.2	10.95	6.2	6.4	0.2
C7	12.2	6.3	6.2	−0.1	10.98	6.3	6.2	−0.1
C3	12.1	6.2	6.0	−0.2	11.14	6.4	6.0	−0.4
C4	12.0	6.2	5.7	−0.5	11.13	6.4	5.7	−0.7
C9	11.3	5.4	5.5	0.1	11.19	6.5	5.5	−1
C14	12.4	6.6	5.4	−1.2	11.10	6.4	5.4	−1
C5	11.6	5.7	5.3	−0.4	10.23	5.5	5.3	−0.2
C13	11.1	5.2	5.2	0	9.27	4.6	5.2	0.6
C6	11.9	6.0	5.0	−1	10.45	5.7	5.0	−0.7
C12	11.4	5.6	5.0	−0.6	10.12	5.4	5.0	−0.4
C11	11.6	5.8	4.9	−0.9	10.34	5.6	4.9	−0.7
C10	11.8	5.9	4.8	−1.1	10.37	5.7	4.8	−0.9

[a]The maximum possible fit score is 15; the error of the prediction is given as the difference between experimental and estimated pK_i values.

Structural Model of the AT_1 Receptor. Figure 3 shows a phylogenetic tree of the human AT_1R and all class A GPCRs with known structure. It can be seen in the figure that AT_1R is located in a branch that includes opioid receptors (OPRX, OPRK, OPRD, and OPRM), the protease-activated receptor (PAR1), the neurotensin receptor (NTR1), and the chemokine CXCR4 receptor, with the latter being clearly the most closely related receptor. Figure 4 shows the superimposition of different AT_1 receptor models that were constructed based on the crystal structures of either rhodopsin, β_2, $S1P_1R$, or CXCR4 as the representative structures for the most relevant branches obtained in the cluster analysis. The figure illustrates pictorially that all homology models mostly retain analogous secondary/tertiary structures at the seven-helical-bundle domain. However, it can be seen that the orientation of $Y87^{2.63}$, $R167^{4.64}$, and $K199^{5.42}$, three of the key side chains in the binding pocket, vary significantly depending on the used template. TM 2 of CXCR4 adopts a closed helical segment (3_{10} helix or tight turn), rhodopsin and β_2- have an open helical segment (π bulge or wide turn), and $S1P_1R$ adopts a canonical helix.[45] This different conformation of TM 2 is responsible for the change in the localization of the side chains of residues at the extracellular side (Figure 4), which makes $Y87^{2.63}$ to point toward the helical bundle only in the CXCR4-based model of AT_1R. Both AT_1R and CXCR4 contain the $(S/T)xP^{2.58}$ motif that has been described as a key modulator of TM 2.[46,47] Similarly, the additional helical turn of TM 4 in CXCR4 (the helix extends up to position 4.64), together with the two β-strands that form the second extracellular loop (ECL2) of CXCR4 and other receptors binding peptide ligands,[48] shift the extracellular part of TM 4 toward TM 3 (~3 Å). In contrast to the other templates, this conformation of TM 4 positions the key $R167^{4.64}$ side chain, which has been shown to be involved in angiotensin II, losartan, EXP3174, and candesartan binding,[49] at the center of the helical bundle and, thus, forming the binding site crevice (Figure 4). All receptors with an available crystal structure except the $S1P_1R$ exhibit a π-bulge or wide turn in TM 5 that is characteristic of $P^{5.50}$-containing receptors.[50] Models based on these receptors position $K199^{5.42}$ toward the binding site (Figure 4). Mutation of $K199^{5.42}$ significantly reduces the binding affinity of nonpeptide antagonists and fully impedes the

dx.doi.org/10.1021/ci400400m | J. Chem. Inf. Model. XXXX, XXX, XXX−XXX

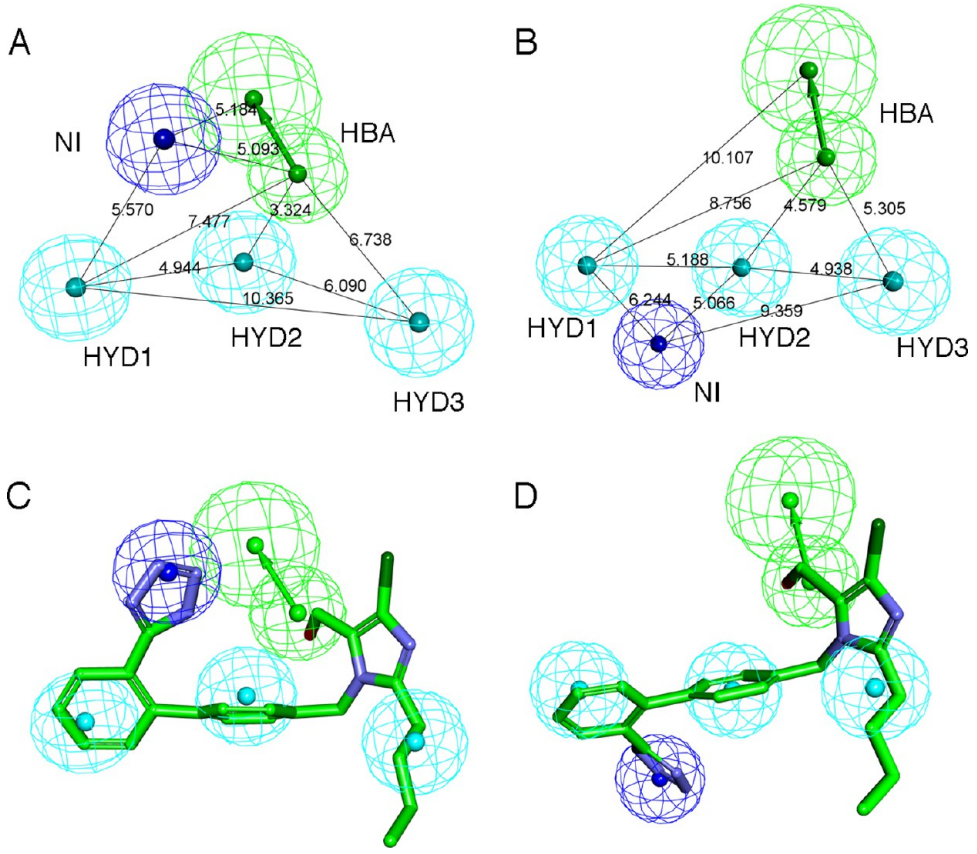

Figure 2. Pharmacophore hypotheses 1 (panels **A** and **C**) and 2 (panels **B** and **D**) for the compounds depicted in Table 1. The structural features are a negatively ionizable group (NI, blue), a hydrogen bond acceptor group (HBA, green), and three hydrophobic sites (HYD1-HYD3, cyan). Each feature is drawn as single globes except for HBA, where an extra globe indicates the directional nature of this chemical function. **A, B**) Pharmacophore models with the relative distances between features (in Å). **C, D**) Same pharmacophore models with the structure of Losartan mapped onto the hypotheses 1 and 2.

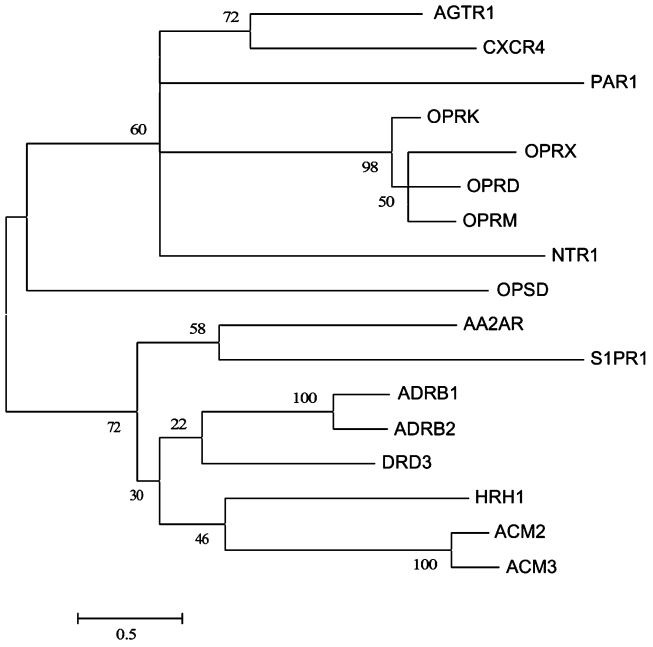

Figure 3. Phylogenetic tree for all class A GPCRs with known structure plus the human AT_1R. Analysis was made with MEGA5 software,[68] using the maximum likelihood method under the JJT+G+I+F pairwise distance model[69] between the amino acid sequences. Values at each ramification correspond to the bootstrap percentages.[70]

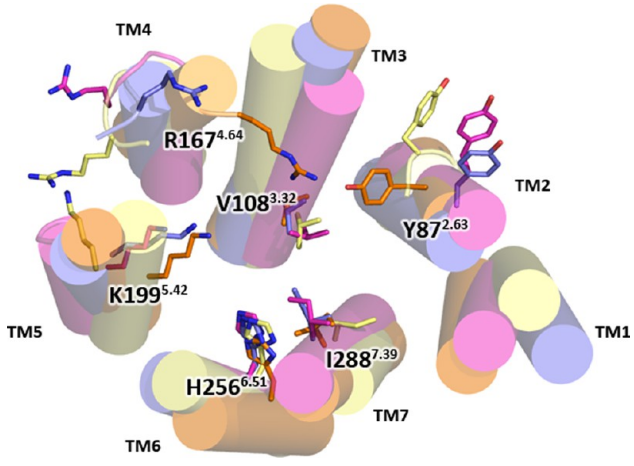

Figure 4. TM domain comparison of AT_1R homology models built using the crystal structures of rhodopsin (magenta), β_2-adrenergic (blue), $S1P_1R$ (yellow), and CXCR4 (orange) receptors. Helices are represented as cylinders, and key side chains located in TM 2 ($Y87^{2.63}$), TM 3 ($V108^{3.32}$), TM 4 ($R167^{4.64}$), TM 5 ($K199^{5.42}$), TM 6 ($H256^{6.51}$), and TM 7 ($I288^{7.39}$) are shown as sticks.

binding of angiotensin II.[51] Because the $S1P_1R$ lacks $P^{5.50}$ and exhibits a regular α-helical conformation of TM5, the $S1P_1R$-based model wrongly positions the key $K199^{5.42}$ side chain pointing toward the membrane environment. Thus, CXCR4 was found to fulfill both sequence (Figure 3) and structural (Figure 4) characteristics and was used to model AT_1R (see Methods).

dx.doi.org/10.1021/ci400400m | J. Chem. Inf. Model. XXXX, XXX, XXX−XXX

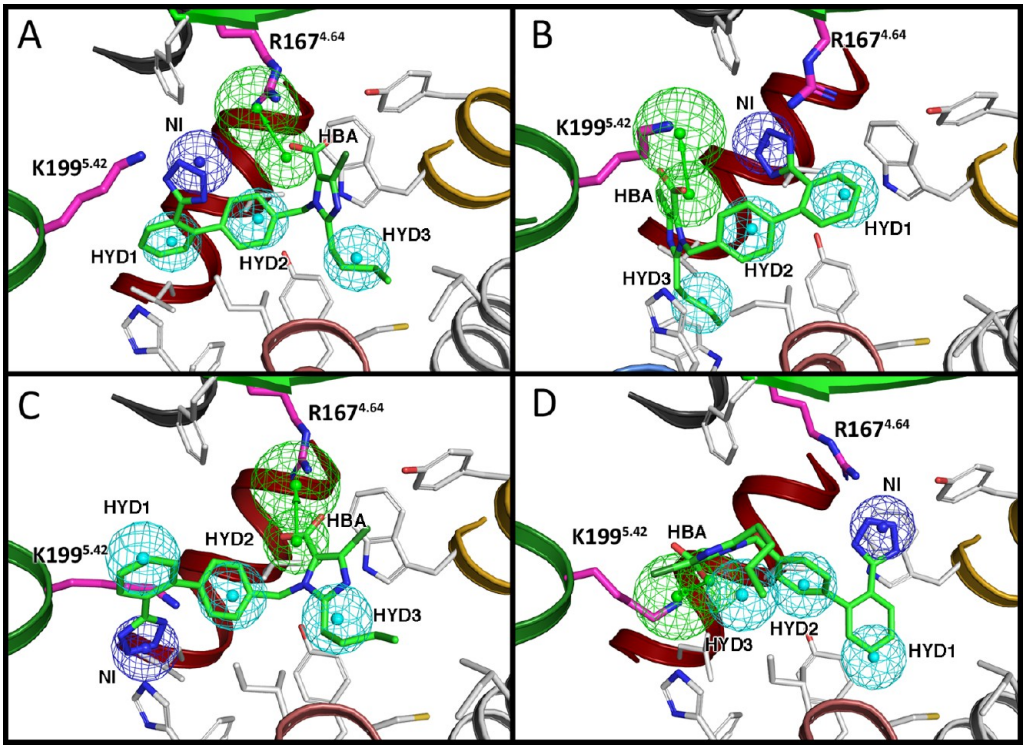

Figure 5. The four main docking poses depicted for EXP3174 as a representative case. All ligands were docked into AT_1R in such a manner that i) the NI pharmacophoric element (blue sphere) either forms an ionic interaction with $K199^{5.42}$ (panels **A** and **C**) or $R167^{4.64}$ (panels **B** and **D**) and ii) HBA (green spheres) either forms a hydrogen bond interaction with $K199^{5.42}$ (panels **B** and **D**) or $R167^{4.64}$ (panels **A** and **C**). Ligands are in either the *syn* (panels **A** and **B**, hypothesis 1) or *anti* (panels **C** and **D**, hypothesis 2) conformation.

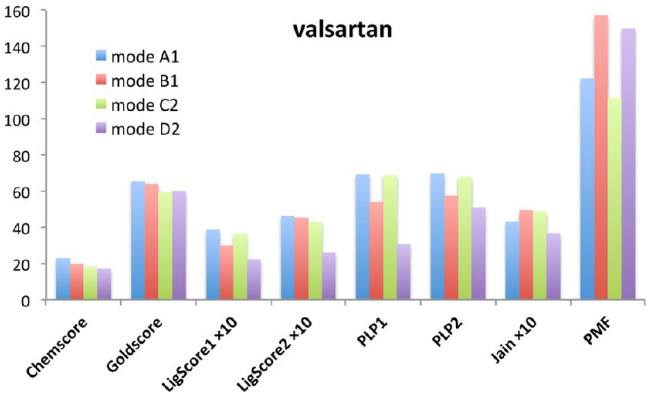

Figure 6. Docking scores for the binding of valsartan to the receptor model, in binding modes A1-D2, evaluated with several scoring functions. Functions LigScore1, LigScore2, and Jain are multiplied by a factor of 10 for comparison and clarity reasons.

Binding AT_1R Antagonists into the Receptor Model. Four different binding modes (A–D) were assessed for sartans and the V series of ligands, arising from the various possible interaction models involving NI and HBA pharmacophoric elements of the ligands (hypotheses 1 and 2) and $R167^{4.64}$ and $K199^{5.42}$ of the AT_1R detailed above. In mode A1 (Figure 5A), the NI pharmacophoric element forms an ionic interaction with $K199^{5.42}$, while HBA (in the *syn* conformation relative to NI, hypothesis 1) forms a hydrogen bond interaction with $R167^{4.64}$. In mode B1 (Figure 5B), NI and HBA are reversed to interact with $R167^{4.64}$ and $K199^{5.42}$, respectively. In modes C2 and D2, the *anti* conformation of the ligand is docked in such a manner that NI interacts with $K199^{5.42}$ and HBA with $R167^{4.64}$ (hypothesis 2, mode C2, Figure 5C) or in the opposite way (hypothesis 2, mode D2, Figure 5D).

Table 3. Experimental and Theoretical Free Energies of Binding, (ΔG^{expt}_{bind}) and (ΔG^{LIE}_{bind}) respectively, Calculated Using the Linear Interaction Energy (LIE) Procedure (see Methods), in Orientations A1, B1, C2, and D2 (See Text and Figure 5), for AT_1R Compounds with K_i < 10 nM

		ΔG^{LIE}_{bind} (kcal/mol)			
compound	ΔG^{expt}_{bind} (kcal/mol)	A1	B1	C2	D2
losartan	−11.3	**−10.0**	−6.9	−7.6	−7.1
eprosartan	−11.0	**−10.5**	−6.8	−7.3	−6.9
EXP3174	−11.9	**−12.2**	−8.7	−11.6	−7.2
valsartan	−11.0	**−11.2**	−6.9	−9.8	−5.9
irbesartan	−12.4	**−11.0**	−5.7	−8.0	−7.0
olmesartan	−12.5	**−11.8**	−6.7	−10.0	−6.5
V8002	−11.7	**−11.4**	−5.3	−8.6	−4.9

High affinity compounds (K_i values <10 nM) were docked into the receptor model using GOLD (see Methods). Each ligand was docked twice using a distance constraint in such a manner that the protonated amine of $K199^{5.42}$ is located within 4 Å from the tetrazole group or from the carboxyl group of the ligands. All docking solutions were visually inspected and the poses corresponding to modes A1, B2, C2, and D2 were extracted, for further evaluation with several scoring functions (see Methods). Generally, binding mode A1 was scored higher in most cases, especially with the scoring functions Goldscore, Chemscore, Ligscore1, and Ligscore2 (Figure S2). In particular, valsartan shows a slight preference for mode A1 in most of the scoring functions, though without significant differences (Figure 6).

dx.doi.org/10.1021/ci400400m | J. Chem. Inf. Model. XXXX, XXX, XXX−XXX

Table 4. Contributions of Each Potential Energy Term (van der Waals; vdW) and (Electrostatic; el) to the Computed Binding Free Energies (ΔG^{LIE}_{bind}) Extracted from the MD Simulations in the Bound and Free States of Each Ligand Expressed in kcal/mol[a]

compound	$\langle U^{vdW}_{l\text{-}s}\rangle_{bound}$	$\langle U^{vdW}_{l\text{-}s}\rangle_{free}$	$\langle U^{el}_{l\text{-}s}\rangle_{bound}$	$\langle U^{el}_{l\text{-}s}\rangle_{free}$	ΔG^{LIE}_{bind}
losartan	−45.5	−29.2	−81.3	−84.2	−10.0
eprosartan	−39.3	−17.6	−168.4	−172.8	−10.5
EXP3174	−23.6	−23.0	−143.8	−143.4	−12.2
valsartan	−42.5	−23.8	−151.0	−154.0	−11.2
irbesartan	−52.8	−33.8	−77.2	−78.3	−11.0
olmesartan	−42.9	−26.3	−142.3	−143.2	−11.8
V8002	−42.2	−21.9	−149.4	−154.3	−11.4

[a]Data shown corresponds to time averages for the simulations with the most favorable orientation (mode A1) for a selected set of AT_1R compounds with K_i < 10 nM. The value of γ employed for the fitting was γ = −9.20 kcal/mol.

Evaluation of the Binding Free Energy through Molecular Dynamics Simulations. The docking solutions corresponding to modes A1, B2, C2, and D2 were refined using MD simulations (see Methods). The LIE method (see Methods) was employed to estimate the free energies of binding for modes A1−D2 (Table 3). Clearly binding modes A1 and C2, in which NI interacts with K199$^{5.42}$ and HBA interacts with R167$^{4.64}$, are more favorable than modes B1 and D1, in which these interactions are reversed. Moreover, binding mode A1, in which the NI element is pointing toward the extracellular environment (*syn* conformation, Figure 5A), is more favorable than binding mode C2, in which the NI element is buried in the binding site crevice (*anti* conformation, Figure 5C). This is attributed to the fact that in binding mode A1 both NI and HBA pharmacophoric elements are exposed to the extracellular bulk water (see below). Notably, the computed binding free energies for binding mode A1 are in the range of the experimentally determined binding free energies (Table 4). However, the LIE method has been useful to discern between the A1−D2 binding modes rather than to predict the differences in experimental binding free energy because they are smaller than the statistical error associated with the computational method. In specific, in binding mode A1, K199$^{5.42}$ anchors the NI pharmacophoric element that is mainly formed by the tetrazole ring (losartan, EXP3174, valsartan, irbesartan, olmesartan, V8002) or the carboxylate group (eprosartan) in the selected set of AT_1R ligands (Figure 7). HYD1 and HYD2 correspond in both cases to the phenyl ring (biphenyl group) that interacts with V108$^{3.32}$, H256$^{6.51}$, and Y292$^{7.43}$. The pharmacophoric HYD3 element corresponding to the propyl or butyl group is placed in a hydrophobic cavity, between TMs 1 and 7, formed by I31$^{1.35}$ and I288$^{7.39}$. Finally, the HBA feature is formed by either −CH_2OH (losartan), >C═O (irbesartan), or >COO^- (eprosartan, EXP3174, valsartan, olmesartan, V8002), which interacts with R167$^{4.64}$. This binding mode contrasts with the proposed interaction of the carboxyl group of candersatan with T287$^{7.38}$.[52] Clearly compounds bearing the negatively charged carboxyl group as HBA form a stronger salt bridge interaction with the positively charged guanidine group of R167$^{4.64}$. An important feature in the binding of losartan, EXP3174, and

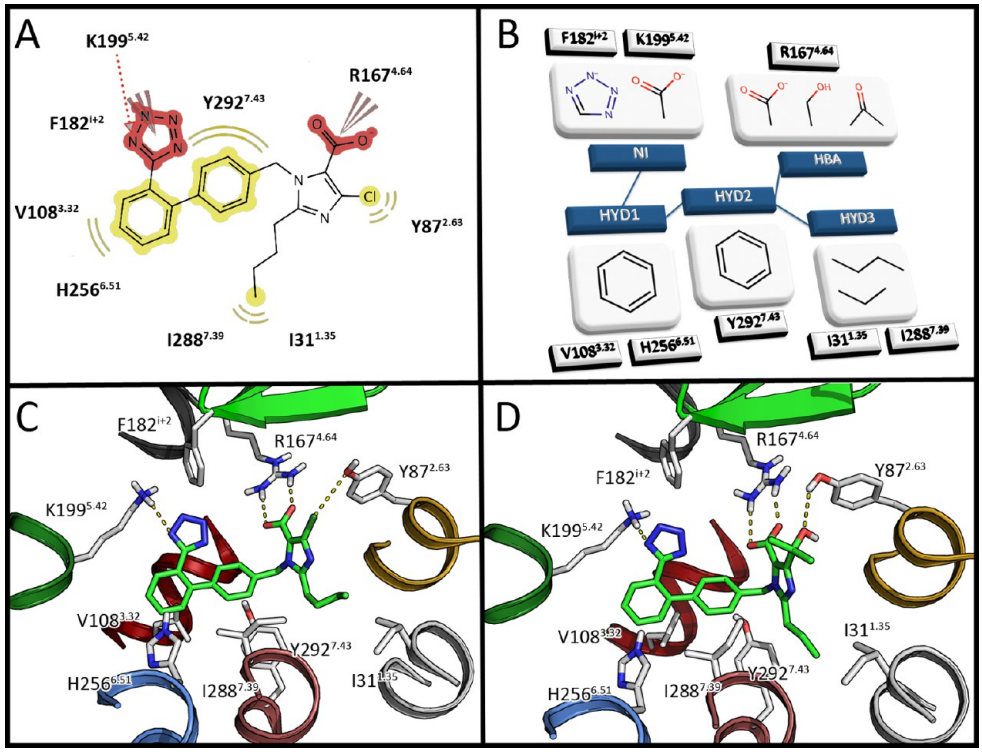

Figure 7. Schematic (**A, B**) and structural (**C, D**) representations for the binding mode A1 of sartans, predicted to be the most stable in the Linear Interaction Energy calculations. (**B**) Schematic representation of the pharmacophore hypothesis 1, the most common functional groups observed in compounds with K_i < 10 nM, and the predicted amino acids in the transmembrane domain of the AT_1R involved in the interaction with the ligands. Representative snapshots of the complex between EXP3174 (**C**) and Olmesartan (**D**) with the AT_1R obtained during the molecular dynamics simulations. The color code of the helices is TM 1 in white, 2 in yellow, 3 in red, 4 in gray, 5 in green, 6 in blue, and 7 in light brown, where EL2 is in light green.

dx.doi.org/10.1021/ci400400m | J. Chem. Inf. Model. XXXX, XXX, XXX−XXX

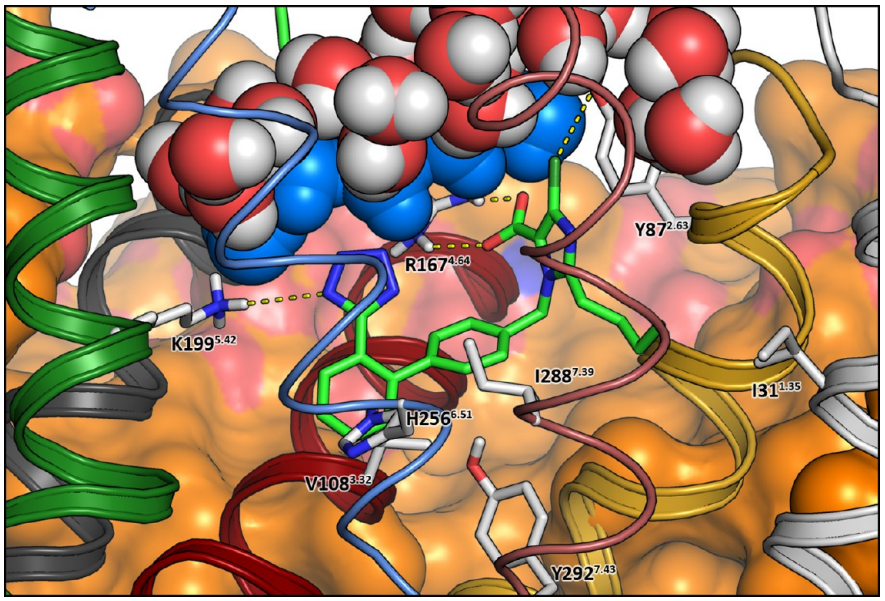

Figure 8. A representative snapshot extracted from the MD simulations of EXP3174/AT_1R showing the accessibility of water molecules to the binding site of the AT_1R. Waters are drawn in vdW spheres with blue color for the inner solvation shell of the ligand. The transmembrane lipids are displayed as orange surface, and the color code of the helices and binding mode of EXP3174 are as in Figure 7.

olmesartan to AT_1R that was not contained in the pharmacophore model, is the additional interaction with Y87$^{2.63}$. Clearly, the hydroxyl group of Y87$^{2.63}$ forms either a halogen bond interaction[53] with the −Cl atom of losartan and EXP3174 or a hydrogen bond interaction with the hydroxyl group of olmesartan. Recent studies have indicated that F182^{i+2}, H183^{i+3}, and Y184^{i+4} in ECL2 (at position i+2, i+3, and i+4, relative to the conserved C180^{i} engaged in a disulfide bond with C115$^{3.25}$ in TM 3) are interacting with angiotensin II.[54] We found that F182^{i+2} is forming an aromatic−aromatic interaction with the tetrazole ring of the ligands.

A crucial contribution to the ligand−receptor binding affinity is, in addition to their electrostatic and van der Waals interactions, the desolvation of the ligand.[55] This is of special relevance in membrane proteins because the ligand has to be transferred from the aqueous environment to the TM binding site crevice.[56] However, in contrast to other GPCRs, the ECL2 of peptide receptors, formed by two β-strands, maintains the binding site rather accessible from the extracellular environment. Thus, the easy exposition of the NI and HBA pharmacophoric elements of the ligands, in the *syn* conformation, to the extracellular environment favors the interactions of the tetrazole or/and the carboxyl groups with bulk water (Figure 8).

CONCLUSIONS

A combination of computer simulations, including pharmacophore modeling, docking, molecular dynamics simulations with explicit inclusion of the membrane and ligand binding free energy calculations, permitted to propose the molecular mechanisms by which sartans interact with AT_1R. A thorough exploration of the binding mode of these ligands by using two pharmacophore hypotheses in combination with four distinct orientations in the receptor's binding pocket suggests a particular interaction pattern. The results are an example of how the repertoire of currently available structural templates for GPCRs in combination with the precise knowledge on helix irregularities within the TM domains can be successfully used to develop molecular models that are useful in the understanding of experimental results. The quality of the models here presented is supported not only for its ability to explain previous experimental results on side-chain substitutions within the binding pocket but also by the agreement between theoretically calculated and experimentally determined ligand-binding free energies. The insights provided for the characterization of the mechanism by which sartans bind to AT_1R may be useful in the design of more potent and selective compounds.

ASSOCIATED CONTENT

Supporting Information

Figure S1: relative energies, calculated at the B3LYP/6-31G* level of theory, of losartan and EXP3174 corresponding to a full rotation of the torsional angle C12−C7−C4-C5. Figure S2: docking scores for binding modes A1, B1, C2, and D2, evaluated with several scoring functions. This material is available free of charge via the Internet at http://pubs.acs.org.

AUTHOR INFORMATION

Corresponding Author

*Phone: +30 2610 997905. Fax: +30 2610 997180. E-mail: ttselios@upatras.gr.

Author Contributions

The manuscript was written through contributions of all authors. All authors have given approval to the final version of the manuscript.

Notes

The authors declare no competing financial interest.

REFERENCES

(1) Smith, R. D.; Timmermans, P. B. Human angiotensin receptor subtypes. *Curr. Opin. Nephrol. Hypertens.* **1994**, *3*, 112−122.

(2) de Gasparo, M.; Catt, K. J.; Inagami, T.; Wright, J. W.; Unger, T. International Union of Pharmacology. XXIII. The angiotensin II receptors. *Pharmacol. Rev.* **2000**, *52*, 415−472.

(3) Steckelings, U. M.; Kaschina, E.; Unger, T. The AT2 receptor - A matter of love and hate. *Peptides* **2005**, *26*, 1401−1409.

(4) Aulakh, G. K.; Sodhi, R. K.; Singh, M. An update on non-peptide angiotensin receptor antagonists and related RAAS modulators. *Life Sci.* **2007**, *81*, 615−639.
(5) Vijayalakshmi, K.; Jananie, R.; Priya, V. Secondary metabolites of *Cynodon dactylon* as an antagonist to angiotensin II type1 receptor: Novel *in silico* drug targeting approach for diabetic retinopathy. *J. Pharmacol. Pharmacother.* **2012**, *3*, 20−25.
(6) Agelis, G.; Roumelioti, P.; Resvani, A.; Durdagi, S.; Androutsou, M.-E.; Kelaidonis, K.; Vlahakos, D.; Mavromoustakos, T.; Matsoukas, J. An efficient synthesis of a rationally designed 1,5 disubstituted imidazole AT_1 angiotensin II receptor antagonist: Reorientation of imidazole pharmacophore groups in losartan reserves high receptor affinity and confirms docking studies. *J. Comput-Aided. Mol. Des.* **2010**, *24*, 749−758.
(7) Maggioni, A. Efficacy of angiotensin receptor blockers in cardiovascular disease. *Cardiovasc. Drugs Ther.* **2006**, *20*, 295−308.
(8) Lew, M. J.; Ziogas, J.; Christopoulos, A. Dynamic mechanisms of non-classical antagonism by competitive AT1 receptor antagonists. *Trends Pharmacol. Sci.* **2000**, *21*, 376−381.
(9) Miura, S.-I.; Fujino, M.; Hanzawa, H.; Kiya, Y.; Imaizumi, S.; Matsuo, Y.; Tomita, S.; Uehara, Y.; Karnik, S. S.; Yanagisawa, H.; Koike, H.; Komuro, I.; Saku, K. Molecular mechanism underlying inverse agonist of angiotensin II type 1 receptor. *J. Biol. Chem.* **2006**, *281*, 19288−19295.
(10) Sica, D.; White, W. B.; Weber, M. A.; Bakris, G. L.; Perez, A.; Cao, C.; Handley, A.; Kupfer, S. Comparison of the novel angiotensin II receptor blocker azilsartan medoxomil vs valsartan by ambulatory blood pressure monitoring. *J. Clin. Hypertens.* **2011**, *13*, 467−472.
(11) Neutel, J. M.; Germino, W. F.; Punzi, H.; McBride, M.; Bryson, C. C.; Belder, R. Results of a double blind placebo controlled study to evaluate the efficacy and safety of PS433540 in human subjects with hypertension. *Circulation* **2008**, *118*, S886−S886.
(12) Yi, S.; Kim, J. W.; Kim, T. E.; Kim, J.; Jun, Y. K.; Choi, J.; Yoon, S. H.; Choi, J. Y.; Song, S. H.; Shin, S. G.; Jang, I. J.; Yu, K. S. Effect of multiple doses of fimasartan, an angiotensin II receptor antagonist, on the steady-state pharmacokinetics of digoxin in healthy volunteers. *Int. J. Clin. Pharm. Ther.* **2011**, *49*, 321−327.
(13) Day, P. W.; Rasmussen, S. G. F.; Parnot, C.; Fung, J. J.; Masood, A.; Kobilka, T. S.; Yao, X.-J.; Choi, H.-J.; Weis, W. I.; Rohrer, D. K.; Kobilka, B. K. A monoclonal antibody for G protein-coupled receptor crystallography. *Nat. Methods* **2007**, *4*, 927−929.
(14) Serrano-Vega, M. J.; Magnani, F.; Shibata, Y.; Tate, C. G. Conformational thermostabilization of the beta1-adrenergic receptor in a detergent-resistant form. *Proc. Natl. Acad. Sci.* **2008**, *105*, 877−882.
(15) Katritch, V.; Cherezov, V.; Stevens, R. C. Diversity and modularity of G protein-coupled receptor structures. *Trends Pharmacol. Sci.* **2012**, *33*, 17−27.
(16) Katritch, V.; Cherezov, V.; Stevens, R. C. structure-Function of the G protein-coupled receptor superfamily. *Annu. Rev. Pharmacol. Toxicol.* **2013**, *53*, 531−556.
(17) Liapakis, G.; Cordomí, A.; Pardo, L. The G-protein coupled receptor family: Actors with many faces. *Curr. Pharm. Des.* **2012**, *18*, 175−185.
(18) Olivella, M.; Gonzalez, A.; Pardo, L.; Deupi, X. Relation between sequence and structure in membrane proteins. *Bioinformatics* **2013**, *29*, 1589−1592.
(19) Hansson, T.; Marelius, J.; Aqvist, J. Ligand binding affinity prediction by linear interaction energy methods. *J. Comput-Aided. Mol. Des.* **1998**, *12*, 27−35.
(20) *Discovery Studio Modeling Environment*, Release 3.5; Accelrys Software Inc.: San Diego, CA, 2012.
(21) Cagigal, E.; Gonzalez, L.; Alonso, R. M.; Jimenez, R. M. pKa determination of angiotensin II receptor antagonists (ARA II) by spectrofluorimetry. *J. Pharm. Biomed. Anal.* **2001**, *26*, 477−486.
(22) Li, H.; Sutter, J.; Hoffman, R. HypoGen: An automated system for generating 3D predictive pharmacophore models. In *Pharmacophore Perception, Development and Use in Drug Design*; Guner, O., Ed.; International University Line: 2000.
(23) Marti-Renom, M. A.; Stuart, A. C.; Fiser, A.; Sanchez, R.; Melo, F.; Sali, A. Comparative protein structure modeling of genes and genomes. *Annu. Rev. Biophys. Biomol. Struct.* **2000**, *29*, 291−325.
(24) Wu, B.; Chien, E. Y. T.; Mol, C. D.; Fenalti, G.; Liu, W.; Katritch, V.; Abagyan, R.; Brooun, A.; Wells, P.; Bi, F. C.; Hamel, D. J.; Kuhn, P.; Handel, T. M.; Cherezov, V.; Stevens, R. C. Structures of the CXCR4 chemokine GPCR with small-molecule and cyclic peptide antagonists. *Science* **2010**, *330*, 1066−1071.
(25) Ballesteros, J. A.; Weinstein, H. Integrated methods for the construction of three-dimensional models and computational probing of structure-function relations in G protein-coupled receptors. In *Methods in Neurosciences*; Stuart, C. S., Ed.; Academic Press: 1995; Vol. *25*, pp 366−428.
(26) Verdonk, M. L.; Cole, J. C.; Hartshorn, M. J.; Murray, C. W.; Taylor, R. D. Improved protein−ligand docking using GOLD. *Proteins: Struct., Funct., Bioinf.* **2003**, *52*, 609−623.
(27) Krammer, A.; Kirchhoff, P. D.; Jiang, X.; Venkatachalam, C. M.; Waldman, M. LigScore: A novel scoring function for predicting binding affinities. *J. Mol. Graphics Modell.* **2005**, *23*, 395−407.
(28) Gehlhaar, D. K.; Verkhivker, G. M.; Rejto, P. A.; Sherman, C. J.; Fogel, D. R.; Fogel, L. J.; Freer, S. T. Molecular recognition of the inhibitor AG-1343 by HIV-1 protease: Conformationally flexible docking by evolutionary programming. *Chem. Biol.* **1995**, *2*, 317−324.
(29) Gehlhaar, D. K.; Bouzida, D.; Rejto, P. A. Reduced dimensionality in ligand-protein structure prediction: Covalent inhibitors of serine proteases and design of site-directed combinatorial libraries. In *Rational Drug Design*; American Chemical Society: 1999; Vol. *719*, pp 292−311.
(30) Jain, A. N. Scoring noncovalent protein-ligand interactions: A continuous differentiable function tuned to compute binding affinities. *J. Comput-Aided. Mol. Des.* **1996**, *10*, 427−440.
(31) Muegge, I.; Martin, Y. C. A general and fast scoring function for protein−ligand interactions: A simplified potential approach. *J. Med. Chem.* **1999**, *42*, 791−804.
(32) Berendsen, H. J. C.; van der Spoel, D.; van Drunen, R. GROMACS: A message-passing parallel molecular dynamics implementation. *Comput. Phys. Commun.* **1995**, *91*, 43−56.
(33) Cordomi, A.; Edholm, O.; Perez, J. J. Effect of force field parameters on sodium and potassium ion binding to dipalmitoyl phosphatidylcholine bilayers. *J. Chem. Theory Comput.* **2009**, *5*, 2125−2134.
(34) Bussi, G.; Donadio, D.; Parrinello, M. Canonical sampling through velocity rescaling. *J. Chem. Phys.* **2007**, *126*, 14101−14107.
(35) Miyamoto, S.; Kollman, P. A. Settle: An analytical version of the SHAKE and RATTLE algorithm for rigid water models. *J. Comput. Chem.* **1992**, *13*, 952−962.
(36) Darden, T.; York, D.; Pedersen, L. Particle mesh Ewald: An N log(N) method for Ewald sums in large systems. *J. Chem. Phys.* **1993**, *98*, 10089−10092.
(37) Lindorff-Larsen, K.; Piana, S.; Palmo, K.; Maragakis, P.; Klepeis, J. L.; Dror, R. O.; Shaw, D. E. Improved side-chain torsion potentials for the Amber ff99SB protein force field. *Proteins: Struct., Funct., Bioinf.* **2010**, *78*, 1950−1958.
(38) Berger, O.; Edholm, O.; Jähnig, F. Molecular dynamics simulations of a fluid bilayer of dipalmitoylphosphatidylcholine at full hydration, constant pressure, and constant temperature. *Biophys. J.* **1997**, *72*, 2002−2013.
(39) Bayly, C. I.; Cieplak, P.; Cornell, W.; Kollman, P. A. A well-behaved electrostatic potential based method using charge restraints for deriving atomic charges: The RESP model. *J. Phys. Chem.* **1993**, *97*, 10269−10280.
(40) Cordomi, A.; Caltabiano, G.; Pardo, L. Membrane protein simulations using AMBER force field and berger lipid parameters. *J. Chem. Theory Comput.* **2012**, *8*, 948−958.
(41) Frisch, M. J.; Trucks, G. W.; Schlegel, H. B.; Scuseria, G. E.; Robb, M. A.; Cheeseman, J. R.; Scalmani, G.; Barone, V.; Mennucci, B.; Petersson, G. A.; Nakatsuji, H.; Caricato, M.; Li, X.; Hratchian, H. P.; Izmaylov, A. F.; Bloino, J.; Zheng, G.; Sonnenberg, J. L.; Hada, M.; Ehara, M.; Toyota, K.; Fukuda, R.; Hasegawa, J.; Ishida, M.; Nakajima, T.; Honda, Y.; Kitao, O.; Nakai, H.; Vreven, T.; Montgomery, J. A., Jr.;

Peralta, J. E.; Ogliaro, F.; Bearpark, M.; Heyd, J. J.; Brothers, E.; Kudin, K. N.; Staroverov, V. N.; Kobayashi, R.; Normand, J.; Raghavachari, K.; Rendell, A.; Burant, J. C.; Iyengar, S. S.; Tomasi, J.; Cossi, M.; Rega, N.; Millam, J. M.; Klene, M.; Knox, J. E.; Cross, J. B.; Bakken, V.; Adamo, C.; Jaramillo, J.; Gomperts, R.; Stratmann, R. E.; Yazyev, O.; Austin, A. J.; Cammi, R.; Pomelli, C.; Ochterski, J. W.; Martin, R. L.; Morokuma, K.; Zakrzewski, V. G.; Voth, G. A.; Salvador, P.; Dannenberg, J. J.; Dapprich, S.; Daniels, A. D.; Ö, F.; Foresman, J. B.; Ortiz, J. V.; Cioslowski, J.; Fox, D. J. *Gaussian~09 Revision A.1*; 2009.

(42) Almlöf, M.; Brandsdal, B. O.; Åqvist, J. Binding affinity prediction with different force fields: Examination of the linear interaction energy method. *J. Comput. Chem.* **2004**, *25*, 1242−1254.

(43) Åqvist, J.; Hansson, T. On the validity of electrostatic linear response in polar solvents. *J. Phys. Chem.* **1996**, *100*, 9512−9521.

(44) Cheng, Y.; Prusoff, W. Relationship between inhibition constant (Ki) and concentration of inhibitor which causes 50 per cent inhibition (I50) of an enzymatic-reaction. *Biochem. Pharmacol.* **1973**, *22*, 3099−3108.

(45) Gonzalez, A.; Cordomí, A.; Caltabiano, G.; Pardo, L. Impact of helix irregularities on sequence alignment and homology modeling of G protein-coupled receptors. *ChemBioChem* **2012**, *13*, 1393−1399.

(46) Govaerts, C.; Blanpain, C.; Deupi, X.; Ballet, S.; Ballesteros, J. A.; Wodak, S. J.; Vassart, G.; Pardo, L.; Parmentier, M. The TXP motif in the second transmembrane helix of CCR5: A structural determinant of the chemokine-induced activation. *J. Biol. Chem.* **2001**, *276*, 13217−13225.

(47) Deupi, X.; Olivella, M.; Govaerts, C.; Ballesteros, J. A.; Campillo, M.; Pardo, L. Ser and Thr residues modulate the conformation of pro-kinked transmembrane alpha-helices. *Biophys. J.* **2004**, *86*, 105−115.

(48) Peeters, M. C.; van Westen, G. J. P.; Li, Q.; IJzerman, A. P. Importance of the extracellular loops in G protein-coupled receptors for ligand recognition and receptor activation. *Trends Pharmacol. Sci.* **2011**, *32*, 35−42.

(49) Takezako, T.; Gogonea, C.; Saad, Y.; Noda, K.; Karnik, S. S. Network leaning" as a mechanism of insurmountable antagonism of the angiotensin II type 1 receptor by non-peptide antagonists. *J. Biol. Chem.* **2004**, *279*, 15248−15257.

(50) Sansuk, K.; Deupi, X.; Torrecillas, I. R.; Jongejan, A.; Nijmeijer, S.; Bakker, R. A.; Pardo, L.; Leurs, R. A structural insight into the reorientation of transmembrane domains 3 and 5 during family A G protein-coupled receptor activation. *Mol. Pharmacol.* **2011**, *79*, 262−269.

(51) Fierens, F. L.; Vanderheyden, P. M.; Gaborik, Z.; Minh, T. L.; Backer, J. P.; Hunyady, L.; Ijzerman, A.; Vauquelin, G. Lys(199) mutation of the human angiotensin type 1 receptor differentially affects the binding of surmountable and insurmountable non-peptide antagonists. *JRAAS* **2000**, *1*, 283−288.

(52) Yasuda, N.; Miura, S.-i.; Akazawa, H.; Tanaka, T.; Qin, Y.; Kiya, Y.; Imaizumi, S.; Fujino, M.; Ito, K.; Zou, Y.; Fukuhara, S.; Kunimoto, S.; Fukuzaki, K.; Sato, T.; Ge, J.; Mochizuki, N.; Nakaya, H.; Saku, K.; Komuro, I. Conformational switch of angiotensin II type 1 receptor underlying mechanical stress-induced activation. *EMBO Rep.* **2008**, *9*, 179−186.

(53) Wilcken, R.; Zimmermann, M. O.; Lange, A.; Joerger, A. C.; Boeckler, F. M. Principles and applications of halogen bonding in medicinal chemistry and chemical biology. *J. Med. Chem.* **2012**, *56*, 1363−1388.

(54) Unal, H.; Jagannathan, R.; Bhat, M. B.; Karnik, S. S. Ligand-specific conformation of extracellular loop-2 in the angiotensin II type 1 receptor. *J. Biol. Chem.* **2010**, *285*, 16341−16350.

(55) Gohlke, H.; Klebe, G. Approaches to the description and prediction of the binding affinity of small-molecule ligands to macromolecular receptors. *Angew. Chem., Int. Ed. Engl.* **2002**, *41*, 2644−2676.

(56) González, A.; Murcia, M.; Benhamú, B.; Campillo, M.; López-Rodríguez, M. L.; Pardo, L. The importance of solvation in the design of ligands targeting membrane proteins. *MedChemComm* **2011**, *2*, 160−164.

(57) Nicolai, E.; Cure, G.; Goyard, J.; Kirchner, M.; Teulon, J.-M.; Versigny, A.; Cazes, M.; Caussade, F.; Virone-Oddos, A.; Cloarec, A. Synthesis and SAR studies of novel triazolopyrimidine derivatives as potent, orally active angiotensin II receptor antagonists. *J. Med. Chem.* **1994**, *37*, 2371−2386.

(58) Poss, M.; Gu, Z.; Ryono, D.; Reid, J.; Siebermcmaster, E.; Spitzmiller, E.; Dejneka, T.; Dickinson, K.; Williams, S.; Moreland, S.; Delaney, C.; Bird, J.; Waldron, T.; Schaeffer, T.; Heldberg, S.; Petrillo, E. 1−4-Substituted indoles - a potent and selective class of angiotensin-II receptor antagonists. *Bioorg. Med. Chem. Lett.* **1994**, *4*, 145−150.

(59) Salimbeni, A.; Canevotti, R.; Paleari, F.; Poma, D.; Caliari, S.; Fici, F.; Cirillo, R.; Renzetti, A. R.; Subissi, A. N-3-substituted pyrimidinones as potent, orally active, AT1 selective angiotensin II receptor antagonists. *J. Med. Chem.* **1995**, *38*, 4806−4820.

(60) Agelis, G.; Resvani, A.; Durdagi, S.; Spyridaki, K.; Tůmová, T.; Slaninova, J.; Giannopoulos, P.; Vlahakos, D.; Liapakis, G.; Mavromoustakos, T.; Matsoukas, J. The discovery of new potent non-peptide angiotensin II AT1 receptor blockers: A concise synthesis, molecular docking studies and biological evaluation of N-substituted 5-butylimidazole derivatives. *Eur. J. Med. Chem.* **2012**, *55*, 358−374.

(61) Kim, K.; Qian, L.; Bird, J.; Dickinson, K.; Moreland, S.; Schaeffer, T.; Waldron, T.; Delaney, C.; Weller, H.; Miller, A. Quinoxaline N-oxide containing potent angiotensin-II receptor antagonists - synthesis, biological properties, and structure-activity-relationships. *J. Med. Chem.* **1993**, *36*, 2335−2342.

(62) Wexler, R. R.; Greenlee, W. J.; Irvin, J. D.; Goldberg, M. R.; Prendergast, K.; Smith, R. D.; Timmermans, P. B. M. W. M. Nonpeptide angiotensin II receptor antagonists: The next generation in anti-hypertensive therapy. *J. Med. Chem.* **1996**, *39*, 625−656.

(63) Wong, P. C.; Price, W. A.; Chiu, A. T.; Duncia, J. V.; Carini, D. J.; Wexler, R. R.; Johnson, A. L.; Timmermans, P. B. Nonpeptide angiotensin II receptor antagonists. XI. Pharmacology of EXP3174: An active metabolite of DuP 753, an orally active antihypertensive agent. *J. Pharmacol. Exp. Ther.* **1990**, *255*, 211−217.

(64) Bhuiyan, M. A.; Hossain, M.; Miura, S.-i.; Nakamura, T.; Ozaki, M.; Nagatomo, T. Constitutively active mutant N111G of angiotensin II type 1 (AT1) receptor induces homologous internalization through mediation of AT1-receptor antagonist. *J. Pharmacol. Sci.* **2009**, *111*, 227−234.

(65) Murugesan, N.; Tellew, J. E.; Gu, Z.; Kunst, B. L.; Fadnis, L.; Cornelius, L. A.; Baska, R. A. F.; Yang, Y.; Beyer, S. M.; Monshizadegan, H.; Dickinson, K. E.; Panchal, B.; Valentine, M. T.; Chong, S.; Morrison, R. A.; Carlson, K. E.; Powell, J. R.; Moreland, S.; Barrish, J. C.; Kowala, M. C.; Macor, J. E. Discovery of n-isoxazolyl biphenylsulfonamides as potent dual angiotensin II and endothelin a receptor antagonists. *J. Med. Chem.* **2002**, *45*, 3829−3835.

(66) Ferrario, C. M.; Smith, R. D. Role of olmesartan in combination therapy in blood pressure control and vascular function. *Vasc. Health Risk Manage.* **2010**, *6*, 701−709.

(67) Salimbeni, A.; Canevotti, R.; Paleari, F.; Bonaccorsi, F.; Renzetti, A. R.; Belvisi, L.; Bravi, G.; Scolastico, C. Nonpeptide angiotensin II receptor antagonists. synthesis, in vitro activity, and molecular modeling studies of n-[(heterobiaryl)methyl]imidazoles. *J. Med. Chem.* **1994**, *37*, 3928−3938.

(68) Tamura, K.; Peterson, D.; Peterson, N.; Stecher, G.; Nei, M.; Kumar, S. MEGA5: Molecular evolutionary genetics analysis using maximum likelihood, evolutionary distance, and maximum parsimony methods. *Mol. Biol. Evol.* **2011**, *28*, 2731−2739.

(69) Jones, D. T.; Taylor, W. R.; Thornton, J. M. The rapid generation of mutation data matrices from protein sequences. *Comput. Appl. Biosci.* **1992**, *8*, 275−282.

(70) Felsenstein, J. Confidence limits on phylogenies: An approach using the bootstrap. *Evolution* **1985**, *39*, 783−791.